An enhanced identification procedure to determine the rational functions and aerodynamic derivatives of bridge decks

Bartosz Siedziako*, Ole Øiseth

Department of Structural Engineering, Norwegian University of Science and Technology, Trondheim, Richard Birkelands vei 1A, 7491 Trondheim Norway

* *Corresponding author e-mail: bartosz.siedziako@ntnu.no*

Abstract

Development of time-efficient and reliable methods for estimating the aeroelastic properties of bridge decks is of major importance for bridge engineers to make wind tunnel testing more productive and less expensive. This paper presents an enhanced and more efficient procedure to identify rational functions and aerodynamic derivatives from wind tunnel tests of section models. The accuracy of the proposed method was investigated for a wedged shaped box section, a rectangular section with *B*/*D* 1:10 aspect ratio and a twin deck section. In comparison with the data from standard forced vibration tests, the proposed procedure obtained nearly identical results for the eight most influential aerodynamic derivatives. In the case of the twin deck section, the experimental results show that the aerodynamic derivatives are very sensitive to the motion applied and that a linear model therefore cannot uniquely define the self-excited forces for the particular twin deck section tested. The identified results were used to predict the self-excited forces induced under various motion and wind conditions to verify the accuracy of the identified models. Some comments are also given regarding the observed nonlinear effects in the recorded self-excited forces.

Keywords: Rational Functions; Forced Vibration Method; Aerodynamic Derivatives; Random Motion; Wind Tunnel Testing

1 Introduction

Self-excited forces are some of the most important environmental loads for slender, long-span bridges and must be treated carefully to ensure a safe design. Self-excited forces, or aeroelastic forces, are wind-induced, motion-dependent forces that can significantly modify the stiffness and damping properties of the combined structure and flow system. This may lead to the occurrence of destructive aeroelastic phenomena, such as flutter or galloping, that can be responsible for the collapse of a bridge (Fuller et al., 2000). The self-excited forces are commonly described in the frequency domain by aerodynamic derivatives that are functions of reduced velocity and depend on the geometry of the bridge deck (Scanlan and Tomko, 1971).

The aerodynamic derivatives can be identified by means of wind tunnel tests of section models of bridge decks. Compared to the full (Wardlaw, 1980) and taut strip (Scanlan et al., 1997) testing techniques, section model tests has advantages in terms of the scale of the model (Matsuda et al., 2001; Zasso et al., 2014), which implies that the tests can be conducted in wind tunnels of a reasonable size and with lower costs. Therefore, the section model testing technique is an ideal tool for early design. However, the standard methods for estimating aerodynamic derivatives with a use of forced or free vibration setups require testing the section model under several configurations. Each of the state-of-the-art tests provide experimental results for a single reduced velocity, and since it is important to obtain data at a wide range of reduced velocities, several tests at different motion frequencies and velocities are necessary. Moreover, in the past, P_i^* derivatives describing the self-excited drag, lift and pitching moment due to lateral bridge deck motion were often approximated by applying quasi-steady theory (Boonyapiny et al., 1999; Chen and Kareem, 2003; Jain et al., 1996; Katsuchi et al., 1999; Øiseth et al., 2010). In contrast, the current trend is to also identify these aerodynamic derivatives, since they can play an important role in the estimation of the flutter speed for some cross sections, as shown in several studies (Sarkar et al., 2004; Singh et al. 1996; Zhang and Brownjohn, 2005). At present, section models are commonly tested with three degrees-of-freedom (DoFs), at several motion frequencies and wind velocities. Furthermore, many experiments need to be performed to obtain the full set of aerodynamic derivatives, increasing the overall time spent in the wind tunnel. This is contradictory to the idea that the section model testing technique should be fast and easy to perform, to investigate several possible bridge deck designs. Therefore, the development of time-efficient and reliable methods for estimating the aerodynamic derivatives and of more productive and less expensive wind tunnel tests for section models is of high interest.

Currently, assessment of bridge deck aerodynamics can be examined in a relatively short time using free vibration setups that allow the overall performance of the section model and its critical velocity to be directly observed in the wind tunnel. Although it is difficult to consider more than two vibration modes with free vibration setups, this method usually provides realistic estimates of the complex flutter phenomenon. However, it is sometimes challenging to define the wind speed at which a bridge deck becomes unstable (Andersen et al., 2016). Moreover, aerodynamic derivatives are not extracted from these tests, precluding the possibility to perform more complex multimode flutter or buffeting analyses. Standard forced vibration tests can usually be performed faster, since the frequency of motion can be altered with use of a control system (Diana et al., 2004), while in the free vibration setup, the frequency of motion must be modified manually by changing the mass or stiffness of the section model (Andersen et al., 2015). Moreover, it is known that the forced vibration technique performs more accurately at higher reduced velocities, higher motion amplitudes, increased turbulence intensities, and for cross sections sensitive to vortex shedding (Cao and Sarkar, 2012; Sarkar et al., 2009). Due to repeatability and

straightforward identification procedures, the forced vibration method is also considered to provide more reliable data (Diana, et al., 2015).

In 2005, Chowdhury and Sarkar (2005) introduced the methodology for experimental identification of rational function coefficients from free vibration tests. Seven years later, Cao and Sarkar (2012) presented an algorithm that can be applied when using data from forced vibration experiments. The rational functions are usually indirectly obtained by curve fitting of the real and the imaginary parts of the transfer function expressed in terms of the rational functions to the experimental data of aerodynamic derivatives (Neuhaus et al., 2009). Compared to the more common approach, the methodology proposed by Chowdhury and Sarkar and Cao and Sarkar has the clear advantage that it is not necessary to identify the aerodynamic derivatives before obtaining the rational functions. This is because the methodology directly use the measured time series of the decaying motion when considering free vibration or time series of the measured self-excited forces during forced vibration tests. These identification techniques thus require testing of the section model at fewer wind speeds. However, that methodology still relies on data from rather simple tests with nearly harmonic oscillations. Therefore, the accuracy of the obtained rational functions increases with the number of performed tests.

This paper presents an enhanced identification procedure, based on the work by Chowdhury and Sarkar (2005) and Cao and Sarkar (2012). In the proposed enhanced procedure a more general motion of the section model is used, while the rational functions coefficients are obtained by solving differential equation. The motion applied is a more general three degrees of freedom random motion generated from a rectangular auto-spectral density. This motion makes it possible to study the self-excited forces for a wider range of reduced velocities and thus in principle, to obtain the full set of rational function coefficients by testing a single motion history at only one wind velocity. It is however important to use validation data to verify the identified coefficients. The procedure will anyway further reduce the number of wind tunnel experiments required. The efficacy and accuracy of the proposed identification technique was studied considering three different section models: wedge, rectangular and twin deck. The range of tested reduced frequencies and nondimensional time for these 3 sections were equal to respectively 1.7-14.5 and 2732 for wedge, 1.0-8.5 and 1600 for rectangular, 1.4-11.6 and 2185 for twin deck section models. The identified rational functions are transformed into aerodynamic derivatives and compared with experimental results from the standard forced vibration procedure (Siedziako et al., 2017a). Furthermore, the identified rational functions are used to reproduce the measured aeroelastic loads induced under random motions at several wind velocities to examine the accuracy of the proposed identification method.

2 Identification procedure

The load model proposed by Scanlan and Tomko (1971) is still the most commonly applied method to define aeroelastic forces in bridge aerodynamics

$$
\begin{aligned}
q_{Se,x} &= \frac{1}{2}\rho V^2 B\left(KP_1^* \frac{\dot{r}_x}{V} + KP_2^* \frac{B\dot{r}_\theta}{V} + K^2 P_3^* r_\theta + K^2 P_4^* \frac{r_x}{B} + KP_5^* \frac{\dot{r}_z}{V} + K^2 P_6^* \frac{r_z}{B} \right) \\
q_{Se,z} &= \frac{1}{2}\rho V^2 B\left(KH_1^* \frac{\dot{r}_z}{V} + KH_2^* \frac{B\dot{r}_\theta}{V} + K^2 H_3^* r_\theta + K^2 H_4^* \frac{r_z}{B} + KH_5^* \frac{\dot{r}_x}{V} + K^2 H_6^* \frac{r_x}{B} \right) \\
q_{Se,\theta} &= \frac{1}{2}\rho V^2 B^2\left(KA_1^* \frac{\dot{r}_z}{V} + KA_2^* \frac{B\dot{r}_\theta}{V} + K^2 A_3^* r_\theta + K^2 A_4^* \frac{r_z}{B} + KA_5^* \frac{\dot{r}_x}{V} + K^2 A_6^* \frac{r_x}{B} \right)
\end{aligned}
\tag{1}
$$

Here, V is the mean wind velocity, ρ represents the air density, B denotes the width of the cross section, $K=B\omega/V$ is the reduced frequency of motion, and r_x, r_z, and r_θ are the horizontal, vertical and torsional displacements, respectively. The dimensionless aerodynamic derivatives are depicted by P_n^*, H_n^*, and A_n^*, where $n \in \{1, 2, \ldots 6\}$. The positive directions of the displacements and forces are displayed in Fig. 2.

To describe the self-excited forces in the time domain, the aerodynamic derivatives that are known only at discrete reduced frequencies must be replaced with continuous functions that are suitable for inverse Fourier transforming (Øiseth et al., 2012). In this study, the rational function approximation that originates from the field of aeronautics is used (Karpel, 1981; Roger, 1977). Eq (2) shows the transfer function for the self-excited forces expressed by means of the rational functions with one lag term to calculate the self-excited forces. One lag term is considered in this study, since is considered to be sufficient for many cross sections , see for instance (Chowdhury and Sarkar, 2005; Neuhaus et al., 2009; Siedziako and Øiseth, 2017). Using more lag terms makes the expression more flexible. However, it increases also a risk that the obtained results perform poor outside the tested range of reduced velocities. It is therefore recommended to use as few lag terms as possible to avoid overfitting. One lag term is often sufficient (Chowdhury and Sarkar, 2005; Neuhaus et al., 2009; Siedziako and Øiseth, 2017) and adding more terms does not improve the results presented in this paper significantly either. It is however, worth to mention that more lag terms can be necessary if one needs to cover a wider reduced velocity range. For the sake of simplicity, this derivation concerns only the lift force; however, similar formulas can be analogously derived for the drag force and pitching moment. The transfer function of the lift force due to vertical motion reads.

$$
\mathbf{F}_z(\omega) = \frac{1}{2}\rho V^2 \left[\mathbf{a}_1 + \mathbf{a}_2 \frac{i\omega B}{V} + \mathbf{a}_3 \left(\frac{i\omega B}{V} \right)^2 + \frac{\mathbf{a}_4\, i\omega B / V}{i\omega B / V + d_z} \right] \tag{2}
$$

Here, the one by three vectors $\mathbf{a}_k$ $k \in \{1 \ldots 4\}$ contain rational function coefficient, while d_z comprises the lag coefficient related to the lift force. The matrix $\mathbf{a}_3$ is associated with the aerodynamic mass that is commonly neglected in bridge aerodynamics and therefore not considered further. By taking the inverse Fourier transform of the transfer function given by Eq. (2), the following time domain expressions for the self-excited lift force can be obtained:

$$q_{Se,z}(t) = \frac{1}{2}\rho V^2 \left(\mathbf{a}_1 \mathbf{r}(t) + \frac{B}{V}\mathbf{a}_2 \dot{\mathbf{r}}(t) + \mathbf{a}_4 \left(\mathbf{r}(t) - \frac{d_z V}{B} \int_0^t e^{-d_z V/B(t-\tau)} \mathbf{r}(\tau) d\tau \right) \right) \tag{3}$$

It can be seen that the time domain representation of self-excited drag contains convolution integrals and it is convenient to define the following variable **Z**(t):

$$\mathbf{Z}(t) = \mathbf{r}(t) - \frac{d_z V}{B} \int_0^t e^{-d_z V/B(t-\tau)} \mathbf{r}(\tau) d\tau \tag{4}$$

This variable can be evaluated with first-order differential equations, obtained by taking the derivative of Eq. (4) as shown by several authors (Chen et al., 2000b; Høgsberg et. al., 2000; Mishra et. al., 2008; Øiseth et al. 2012):

$$\dot{\mathbf{Z}}(t) = \dot{\mathbf{r}}(t) - \frac{d_z V}{B}\mathbf{Z}(t) \tag{5}$$

The Eq. (3) can be simplified by introducing **Z**(t):

$$q_{Se,z}(t) = \frac{1}{2}\rho V^2 \left(\mathbf{a}_1 \mathbf{r}(t) + \frac{B}{V}\mathbf{a}_2 \dot{\mathbf{r}}(t) + \mathbf{a}_4 \mathbf{Z}(t) \right) \tag{6}$$

Then, by differentiating Eq. (6) and replacing $\dot{\mathbf{Z}}(t)$ term with Eq. (5), the following expression can be obtained:

$$\dot{q}_{Se,z}(t) = \frac{1}{2}\rho V^2 \left(\left(\mathbf{a}_1 + \mathbf{a}_4\right)\dot{\mathbf{r}}(t) + \frac{B}{V}\mathbf{a}_2 \ddot{\mathbf{r}}(t) - \mathbf{a}_4 \frac{d_z V}{B}\mathbf{Z}(t) \right) \tag{7}$$

Rewriting Eq. (6), the variable **Z**(t) can be expressed as:

$$\mathbf{a}_4 \mathbf{Z}(t) = -\mathbf{a}_1 \mathbf{r}(t) - \frac{B}{V}\mathbf{a}_2 \dot{\mathbf{r}}(t) + q_{Se,z}(t)\frac{2}{\rho V^2} \tag{8}$$

Inserting Eq. (8) into Eq. (7) yields an expression that can be used to fit rational function coefficients to experimental data.

$$\dot{q}_{Se,z}(t) = \frac{1}{2}\rho V^2 \left(\left(\mathbf{a}_1 + \mathbf{a}_4\right)\dot{\mathbf{r}}(t) + \frac{B}{V}\mathbf{a}_2 \ddot{\mathbf{r}}(t) + \frac{d_z V}{B}\left(\mathbf{a}_1 \mathbf{r}(t) + \frac{B}{V}\mathbf{a}_2 \dot{\mathbf{r}}(t) \right) \right) - \frac{d_z V}{B} q_{Se,z}(t) \tag{9}$$

The same expression has been obtained by Cao and Sarkar (2012) who determined the rational function coefficients by using linear regression. The regression problem was expressed as

$$\dot{\mathbf{q}}_z = \boldsymbol{\psi}\mathbf{X} \tag{10}$$

Here the vector $\dot{\mathbf{q}}_z$ contains the observed values of the derivative of vertical self-excited force; the matrix $\mathbf{X}$ contains the values of the independent variables, namely scaled displacements, velocities and accelerations of the section model. The time histories of the latter ones were obtained with a finite difference method. The vector $\boldsymbol{\psi}$ contains the unknown coefficients.

$$\boldsymbol{\psi} = \left[d_z\mathbf{a}_1,\ \mathbf{a}_1 + \mathbf{a}_4 + d_z\mathbf{a}_2,\ \mathbf{a}_2,\ d_z \right] \qquad \mathbf{X} = \begin{bmatrix} \dfrac{\rho V^3}{2B}\mathbf{r} \\ \dfrac{\rho V^2}{2}\dot{\mathbf{r}} \\ \dfrac{\rho BV}{2}\ddot{\mathbf{r}} \\ -\dfrac{V}{B}\mathbf{q}_z \end{bmatrix} \tag{11}$$

Then to find vector $\boldsymbol{\psi}$ an algorithm that minimizes the sum of squares between measured and predicted values of $\dot{\mathbf{q}}_z$ was applied.

$$\boldsymbol{\psi} = \left(\dot{\mathbf{q}}_z\mathbf{X}^T\right)\left(\mathbf{X}\mathbf{X}^T\right)^T \tag{12}$$

The methodology outlined above has been applied successfully for harmonic motions by Cao and Sarkar (2012). However, we encountered some challenges for the cases we considered, because measurement noise and higher order effects are amplified when taking the derivative of the measured self-excited forces. Filtering the time series after taking the derivative solves this problem when considering single harmonic motion, but it is more challenging to deal with when considering a more general motion. The main reason for the problems observed is the fact that Eq.(9) does not fully hold when the measured self-excited forces depends on the independent variables in a way that cannot be explained by the applied model. In other words the vector $\mathbf{q}_z$ in matrix $\mathbf{X}$, used as an input should contain the values of predicted (based on obtained $\boldsymbol{\psi}$ vector) lift force rather than values measured during experiments. This creates a problem since the predictions are unknown prior to applying Eq. (12) The least squares method applied in Eq. (12) yields therefore accurate results only, when corresponding values of $\boldsymbol{\psi}$ reproduce measured during wind tunnel tests values of the lift force exactly, which is not the case in this study. We suggest therefore to slightly improving this identification technique by making sure that the input lift force correspond to predicted values of this force component. To ensure this Eq. (9) can be modelled as an ordinary differential equation or rewritten into state space form. Then $\boldsymbol{\psi}$ vector can be obtained by fitting coefficients to first order differential equation or through identification of the state space model. Those are demanding computational tasks that are subjects of extensive studies resulting in sophisticated methods for parameter estimation of dynamic systems; see for example (Keesma, 2011; Lim

and Longman, 1998; Ljung, 1987; Schön et. al., 2011). In this study a differential equation solver implemented in MATLAB as one of its built-in functions was used to identify state space model following example given in ("Estimation, Represent Nonlinear Dynamics Using MATLAB File for Grey-Box," 2017). As an initial estimate of $\boldsymbol{\psi}$ the results from the linear regression applying were used. More on identification state space model for the purpose of bridge aerodynamics can be found in (Øiseth, 2015).

Having final estimate of $\boldsymbol{\psi}$ the rational function coefficients can be estimated solving simple system of equations based on Eq. (11). To validate the identification procedure described above, the identified rational functions were converted to aerodynamic derivatives based on transfer function in Eq. (2). The aerodynamic derivatives defining the lift force can be expressed as:

$$\begin{aligned} H_6^* &= real(\mathbf{F}_{z,1})/K^2, \quad H_4^* = real(\mathbf{F}_{z,2})/K^2, \quad H_3^* = real(\mathbf{F}_{z,3})/K^2 \\ H_5^* &= imag(\mathbf{F}_{z,1})/K^2, \quad H_1^* = imag(\mathbf{F}_{z,2})/K^2, \quad H_2^* = imag(\mathbf{F}_{z,3})/K^2 \end{aligned} \tag{13}$$

The framework presented above was first validated by performing numerical wind tunnel tests of sections with known aerodynamic derivatives and rational function coefficients. Random motion histories was first generated from assumed spectral densities and the self-excited forces was calculated using the known rational functions. The results showed that it was possible to identify the rational coefficients from the simulated time series if the frequency content of the applied motion covered the reduced frequency range and thus the reduced velocity range of interest.

3 Experimental procedure

3.1 Forced vibration mechanism

A recently developed forced vibration setup (Siedziako et al., 2017a) that is simultaneously capable of measuring the self-excited forces and moving the section model arbitrarily in heaving, swaying and torsional directions is used in this study. The forced vibration rig is situated in the wind tunnel located in the Fluid Mechanics Laboratory at Norwegian University of Science and Technology. It is the largest wind tunnel in Norway, with an 11 m long, 2 m high, 2.7 m wide test section. Fig. 1 shows a picture from the inside of the wind tunnel during testing.

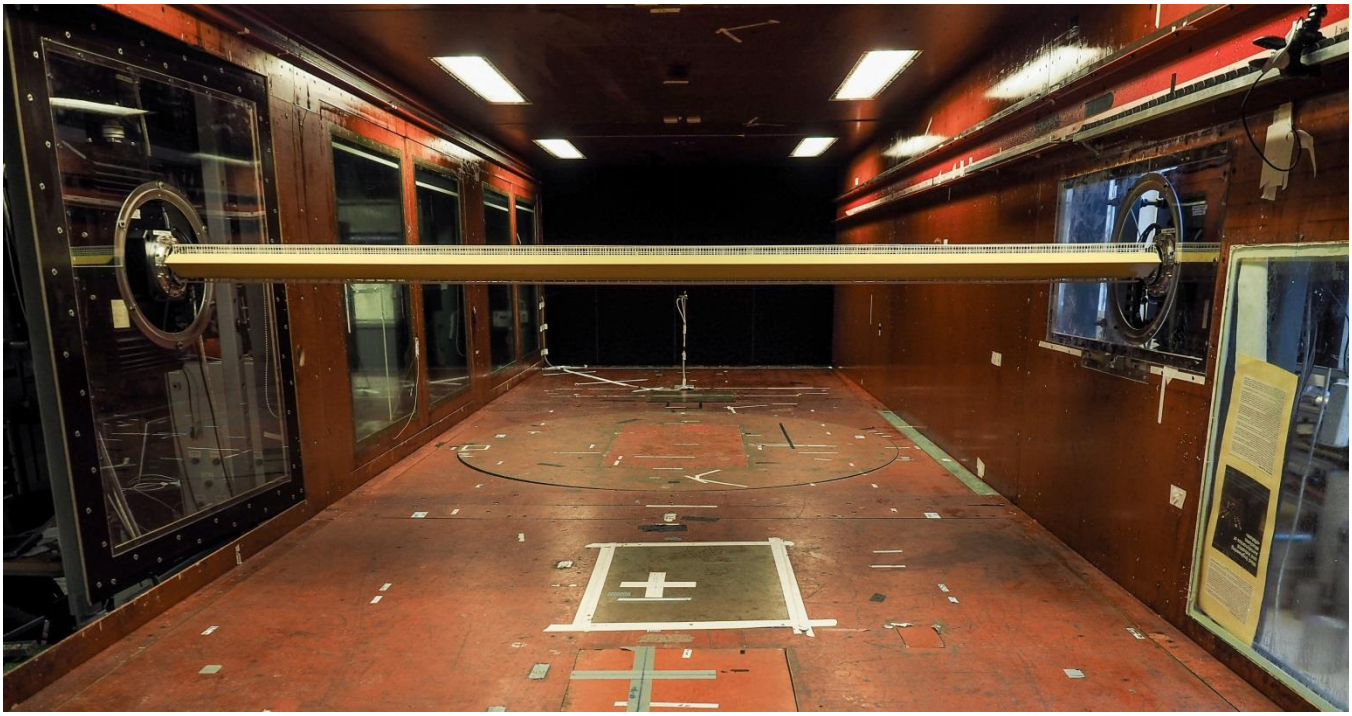

Fig. 1. Experimental setup at NTNU (Siedziako et al., 2017a). The Hardanger Bridge section model mounted between two actuators (photograph by NTNU/K.A. Kvåle).

Two 3-DoFs actuators are the key components of the forced vibration rig. They support the section model at both ends and are mounted on a steel frame outside the wind. The internally connected actuators can to reproduce any uploaded motion of the bridge deck section model in the range ± 10 cm for vertical and horizontal vibrations and ± 90° for rotation. As seen from Fig. 1, the section model is the only component inside the wind tunnel during the experiments.

3.2 Displacement, wind speed and force measurements

The horizontal, vertical and torsional positions of the section model during the experiments are acquired from the encoders on the servomotors. The two 6-DoF's Gamma (by ATI Industrial Automation) load cells measure the forces acting on the bridge deck section models during the wind tunnel experiments. The load cells are located at each side of the wind tunnel and support the section model. Therefore, to find the self-excited forces, the inertia and static contributions need to be separated from the total recorded loads by repeating each test in still-air conditions (Siedziako et al., 2017a). A pitot-static probe placed at the inlet of the wind tunnel was used to measure the mean wind velocity. In this study, all the experiments were conducted in a smooth air flow (Adaramola and Krogstad, 2009). Additionally, recordings from the thermometer inside the wind tunnel allowed the monitoring of the air density due to the change in the temperature during the tests. The sampling rate for the acquired voltage signals was set to 2 kHz, downsampled to 250 Hz when storing the data. More details on the data acquisition and control systems can be found in (Siedziako and Øiseth, 2017b; Siedziako et al., 2017a).

3.3 Section models

Three cross-sectional geometries shown in Fig. 2 were examined in the series of wind tunnel tests with random motion.

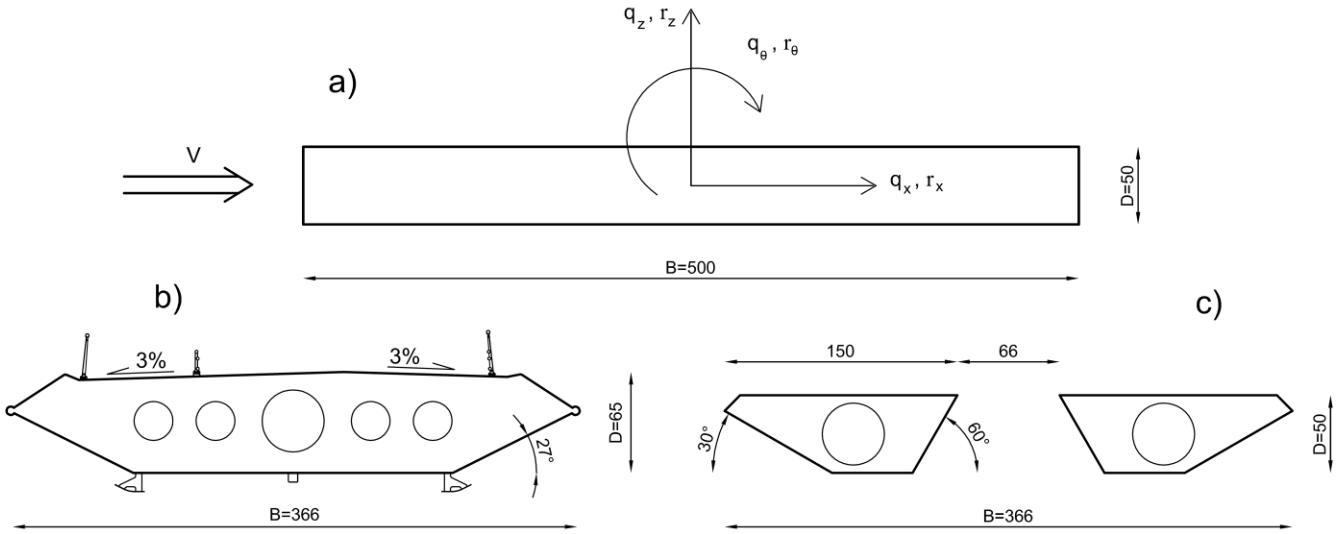

Fig. 2. Cross-sectional dimensions of the bridge deck section model section models used in this study: a) B/D=10 rectangular section, b) detailed Hardanger Bridge section, and c) twin deck section.

A simple rectangular section model with a ratio of B/D=10, a Hardanger Bridge (Fenerci and Øiseth, 2015, 2017; Fenerci et. al., 2017) section model with railings and guide vanes, and a model of a twin box girder were used in this study. An increase in research on twin box girders in recent years motivated the authors of this paper to include this model in the testing program. Although the twin deck section is known to be more resistant to flutter (Andersen et al., 2015, 2016; Yang et al., 2015), the flow pattern around it is somewhat more complex than that of the bluff or streamlined sections. Moreover, a recent study by Skyvulstad et al. (2017) showed that the concept of motion-independent aerodynamic derivatives, which assumes that they are functions of reduced velocity only, might be invalid for some twin deck type geometries. Therefore, it was interesting to examine whether this study would confirm that the aerodynamic derivatives of the chosen twin deck section are sensitive to the motion applied. The aeroelastic properties of the Hardanger Bridge, the longest suspension bridge in Norway, and the twin deck section model used herein had already been evaluated in previous studies conducted at NTNU in (Siedziako and Øiseth, 2017b) and (Skyvulstad et al., 2017), respectively. In this study, in the case of the rectangular section, the aerodynamic derivatives were first identified in the series of single-DoF harmonic forced vibration tests, and then were later compared with the obtained rational functions. The experimental procedure used in this study to extract the aerodynamic derivatives from the standard forced vibration tests can be found in (Siedziako et al., 2017a; Siedziako et. al., 2016).

3.4 Bridge deck motions

The time histories used in this study were generated by Monte Carlo simulations, as described in (Siedziako et al., 2017a). Herein, the designed spectra of the horizontal, vertical and torsional vibrations are rectangular, starting at 0.3 Hz and ending at 2.5 Hz. This ensures that the self-excited forces can be obtained over a wide range of reduced velocities, which is of crucial importance since results obtained outside the covered range might be unreliable. Since the amplitude of the vibrations might have an influence on the identified aerodynamic derivatives, as shown by Chen et al. (2005), three different response magnitudes were considered in this study. The standard deviations of the vertical, horizontal and torsional displacements considered in these tests are shown in Table 1. The length of the time series was 100 seconds, and Fig. 3 shows the first 20 seconds of them.

Test number	Standard deviation of the vibrations		
	r_x [cm]	r_z [cm]	r_θ [°]
1	0.510	0.483	0.938
2	0.350	0.332	0.570
3	0.659	0.639	1.396

Table 1. Standard deviations of the horizontal, vertical and torsional vibrations considered in the wind tunnel tests.

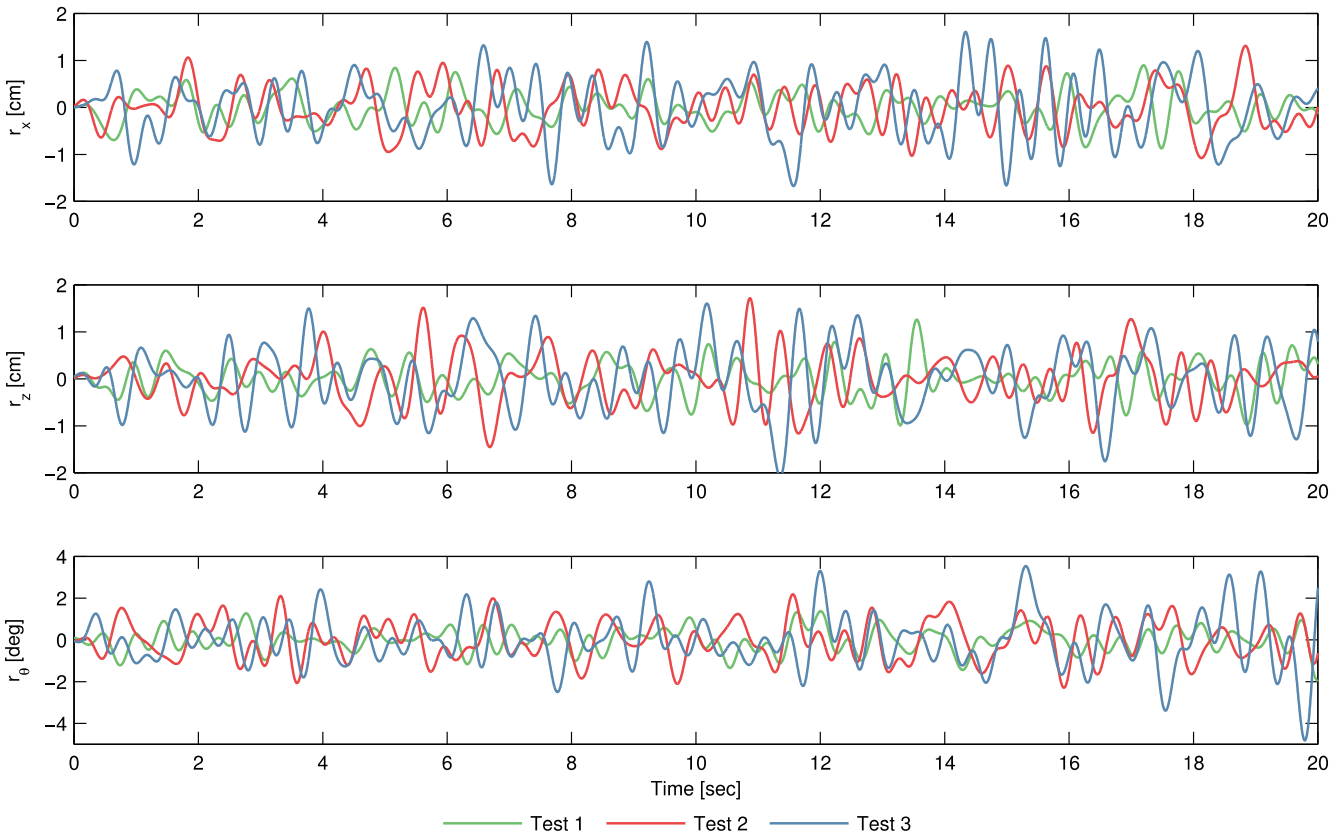

Fig. 3. Part of the time series forced on the section models and used in the identification process.

4 Experimental results and discussion

In order to show the influence of suggested herein enhancement to identification procedure proposed by Cao and Sarkar (2012), standard – Eq. (12) and enhanced identification procedures were used to obtain rational function coefficients. Table 2 compares the fits between measured and predicted self-excited forces, when using linear regression and differential equation solver to find vector $\boldsymbol{\psi}$ containing rational function coefficients. The self-excited forces for this example were recorded, when the twin deck section model was subjected to random vibrations (Test 2) at the mean wind velocity of 4 m/s. It can be seen that predictions of all three self-excited force components have been improved when using suggested herein approach to find rational function coefficients. A distinct increase in the prediction accuracy is observed for the self-excited drag, while only a minor one in case of lift and pitch components. This was expected, since the drag force is usually influenced to a larger extend by the noise due to its low magnitude as well as nonlinear contributions (Chen et al., 2005; Siedziako and Øiseth, 2017b; Xu et al., 2016) that cannot be predicted with a use of applied herein load model. This example demonstrates the efficacy of proposed enhanced identification procedure, although it must be noticed that the improvements in force predictions were less distinct than showed herein in most cases.

Identification method	Drag		Lift		Pitch	
	ρ_{xy}	R^2	ρ_{xy}	R^2	ρ_{xy}	R^2
Least squares – Eq. (12)	0.789	0.489	0.962	0.971	0.919	0.846
Differential equation solver	0.875	0.765	0.980	0.985	0.931	0.868

Table 2. Correlation coefficient (ρ_{xy}) and coefficient of determination (R^2) between measured and predicted self-excited forces, calculated using rational functions obtained applying different identification techniques.

The correlation coefficient and coefficient of determination between the measured (x_i) and predicted (y_i) n-long signals were calculated using Eq. (14) and (15)

$$\rho_{xy} = \frac{\sum_{i=1}^{n} x_i y_i}{\sigma_x \sigma_y n} \tag{14}$$

$$R^2 = 1 - \frac{\sum_{i=1}^{n} (x_i - y_i)^2}{\sum_{i=1}^{n} x_i^2} \tag{15}$$

4.1 Aerodynamic derivatives

The results presented in this paper have been obtained from the wind tunnel tests at 8 and 10 m/s since we consider these tests to be of highest quality because the self-excited forces are large compared to inertia forces. The velocities are perhaps a bit

large if one is interested in the self-excited forces at low mean wind velocities in full scale. The natural frequencies of the first vertical and torsional modes of the Hardanger Bridge are 1 and 2.2 rad/s respectively while the reduced critical flutter velocity is 2.6. The wind tunnel test thus cover the range relevant for buffeting response and flutter analysis in strong winds where the self-excited forces are most relevant. The aerodynamic derivatives obtained using Eq. (13) for the Hardanger Bridge and BD10 section models are presented in Fig. 4 to Fig. 7. The convention proposed by Zasso (1996), where the aerodynamic derivatives related to the velocities and displacements are multiplied by the reduced frequency and reduced frequency squared, respectively is used since it allows a quantitative evaluation of the performance of the proposed identification method.

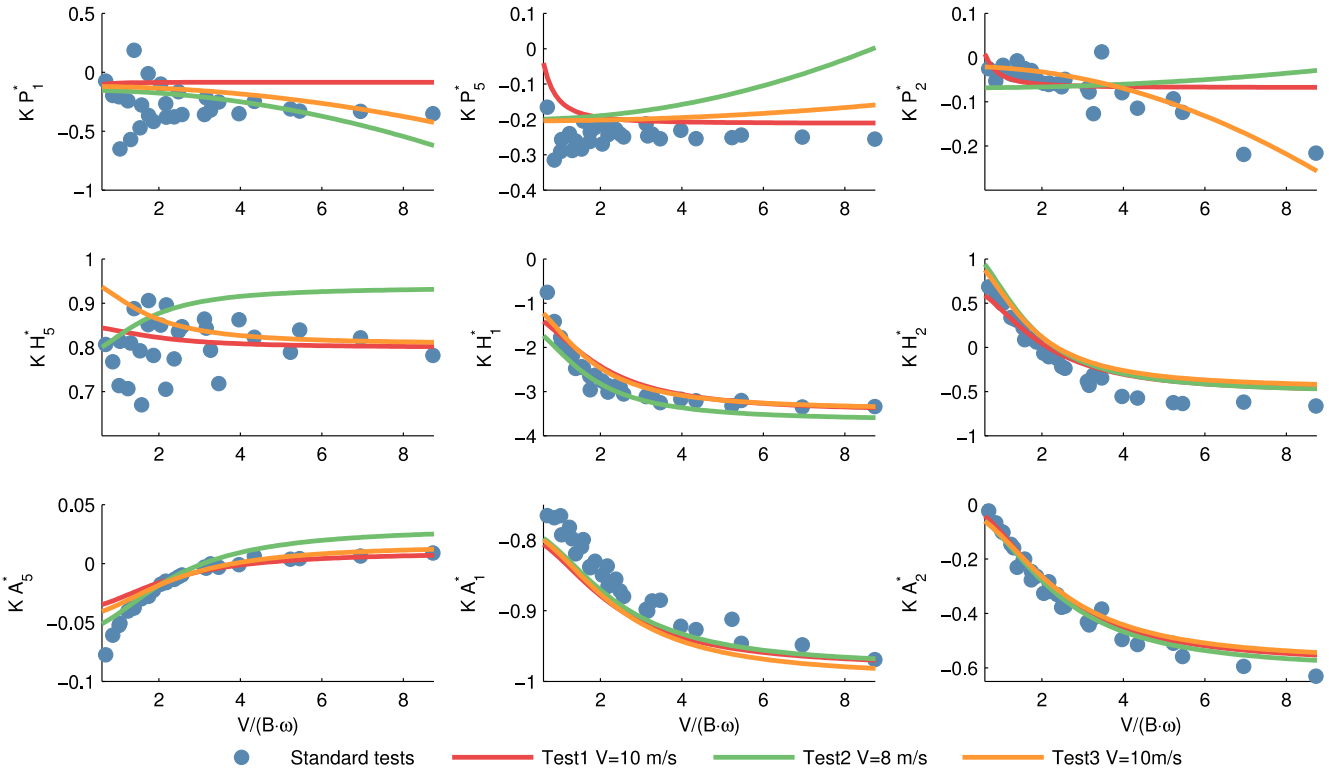

Fig. 4. Aerodynamic derivatives, of the Hardanger Bridge section model, related to the velocities or angular velocities.

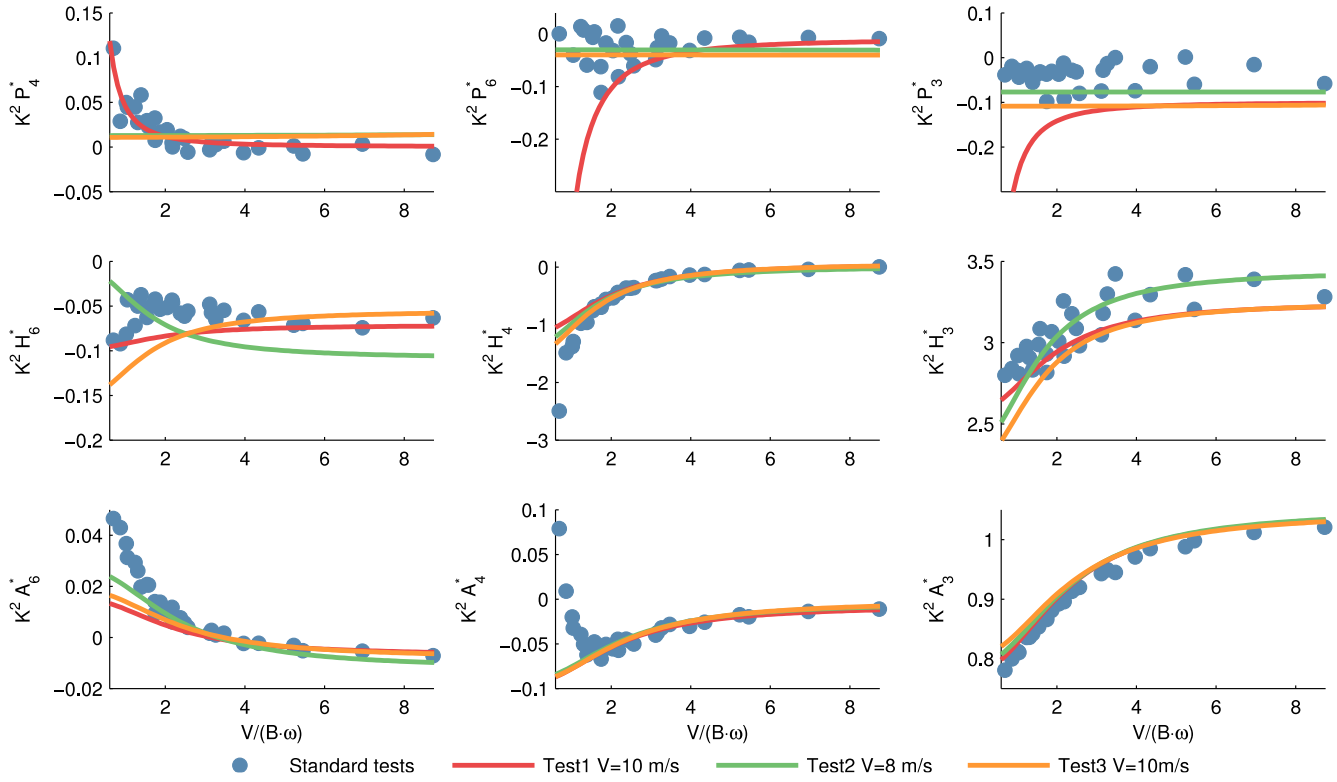

258

259 **Fig. 5.** Aerodynamic derivatives, of the Hardanger Bridge section model, related to the displacements and rotation.

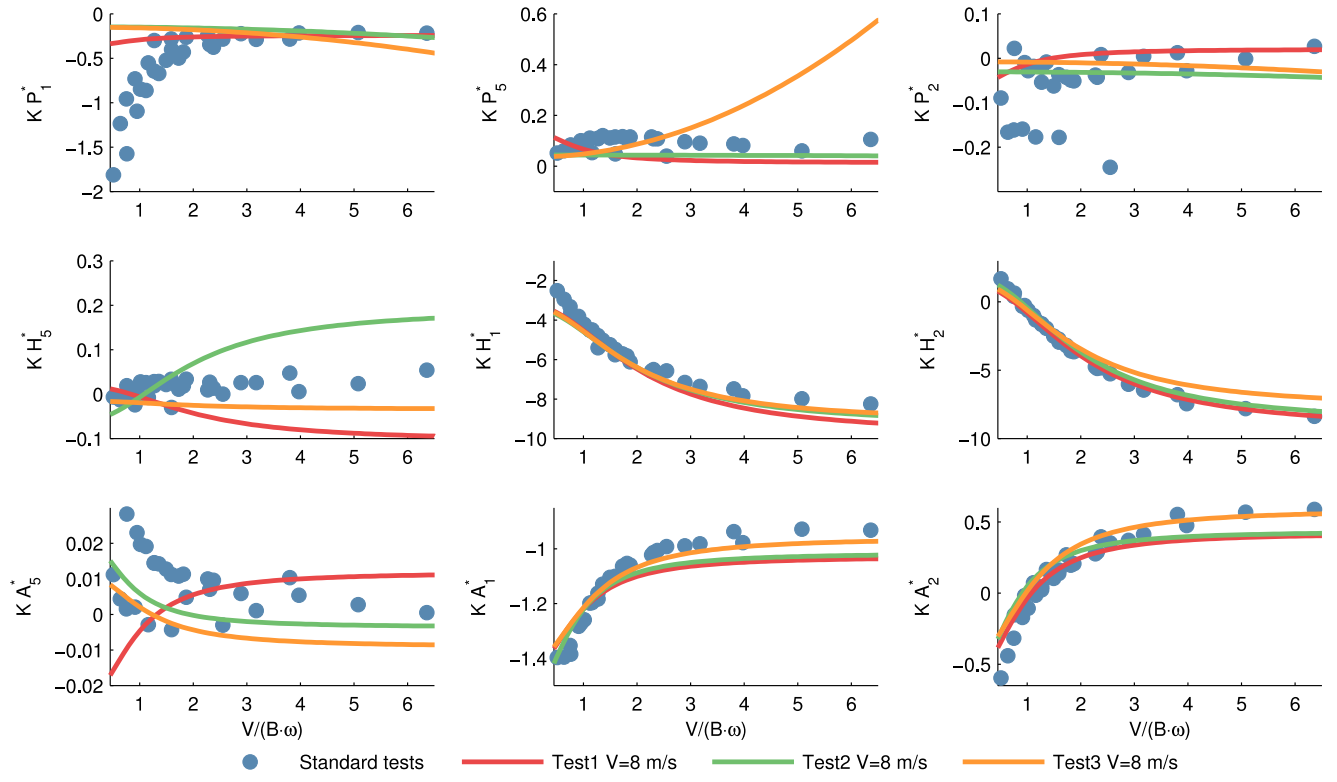

260

Fig. 6. Aerodynamic derivatives, of the rectangular BD10 section model, related to the velocities or angular velocities.

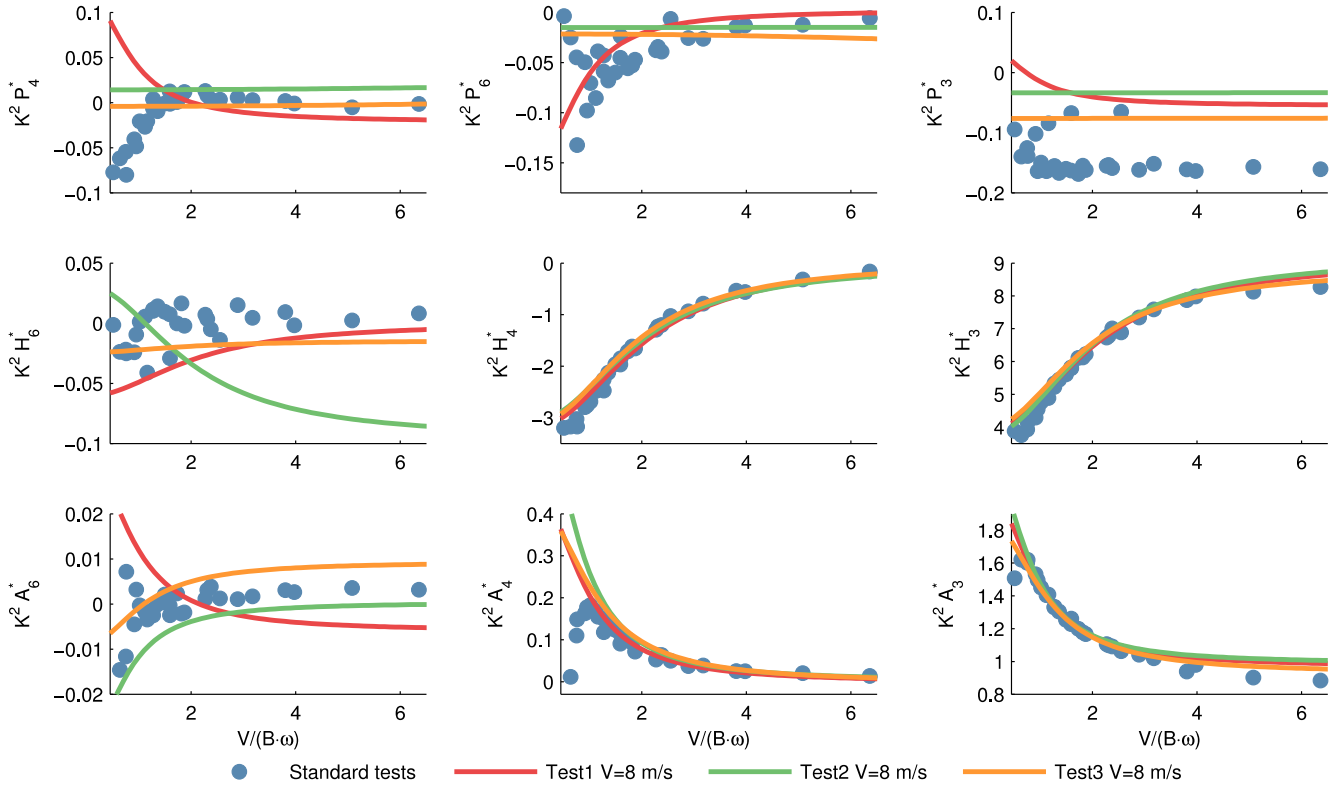

Fig. 7. Aerodynamic derivatives, of the rectangular BD10 section model, related to the displacements and rotation.

For the Hardanger and the rectangular BD10 section models, the obtained aerodynamic derivatives show a very good match with the data obtained in the standard forced vibration tests. Especially for the 8 aerodynamic derivatives considered to be the most influential, namely, A_1^*–A_4^* and H_1^*–H_4^*, the identified results are consistent and nearly identical to the results from the standard tests with 1-DoF harmonic oscillations, represented by the blue dots in Fig. 4 to Fig. 7. Generally, greater discrepancies between the standard forced vibration data and the identified results are observed at higher reduced velocities. This can be attributed to the design of the spectra, uniformly distributed along the frequencies ranging from 0.3 to 2.5 Hz, used to generate the motion histories; this design emphasizes the importance of the self-excited forces induced at the lower reduced velocities, since reduced velocity is inversely proportional to frequency. It is also interesting to study the results in the reduced velocity range not directly covered by the frequency range of the applied motions, which are below 1.45 and below 0.85 for the Hardanger and BD10 sections respectively. The results show that the identified models preforms well for the most important aerodynamic derivatives also in this range. This can partly be attributed to the fact that only one lag term is sued such that abrupt changes in the curves outside the range covered by the applied motion do not occur. The difficulties in finding the aerodynamic derivatives that define the self-excited drag has already been emphasized in a previous study that used the same experimental setup as herein (Siedziako et al., 2017a). Considering the low value of the self-excited drag force

and highly nonlinear behavior of this force component, the results presented here are considered acceptable. Nevertheless, as in the previous studies (Siedziako et al., 2017a; Xu et al., 2016), the results strongly indicate that the load model based on the aerodynamic derivatives is not able to reproduce this force component. P_2^*, P_3^*, P_5^*, and P_6^*, that define the self-excited pitch and lift induced by horizontal motion are also more scattered. However, the forces induced by this motion component are smaller than those generated by the heave or rotation by roughly an order of magnitude, and therefore, are of minor importance.

The aerodynamic derivatives identified for the twin deck section are displayed in Fig. 8 and Fig. 9. Although the results are mostly within range of the results obtained through the standard forced vibration tests, different trends and a large scatter between the separate tests are observed, especially in comparison with the results presented in Fig. 4 to Fig. 7. It is also observed that the results from the standard forced vibration tests do not form consistent trends indicating that a linear model for the self-excited forces is insufficient. The static force coefficients displayed in Fig 10 supports this statement since significant nonlinearities are clearly present.

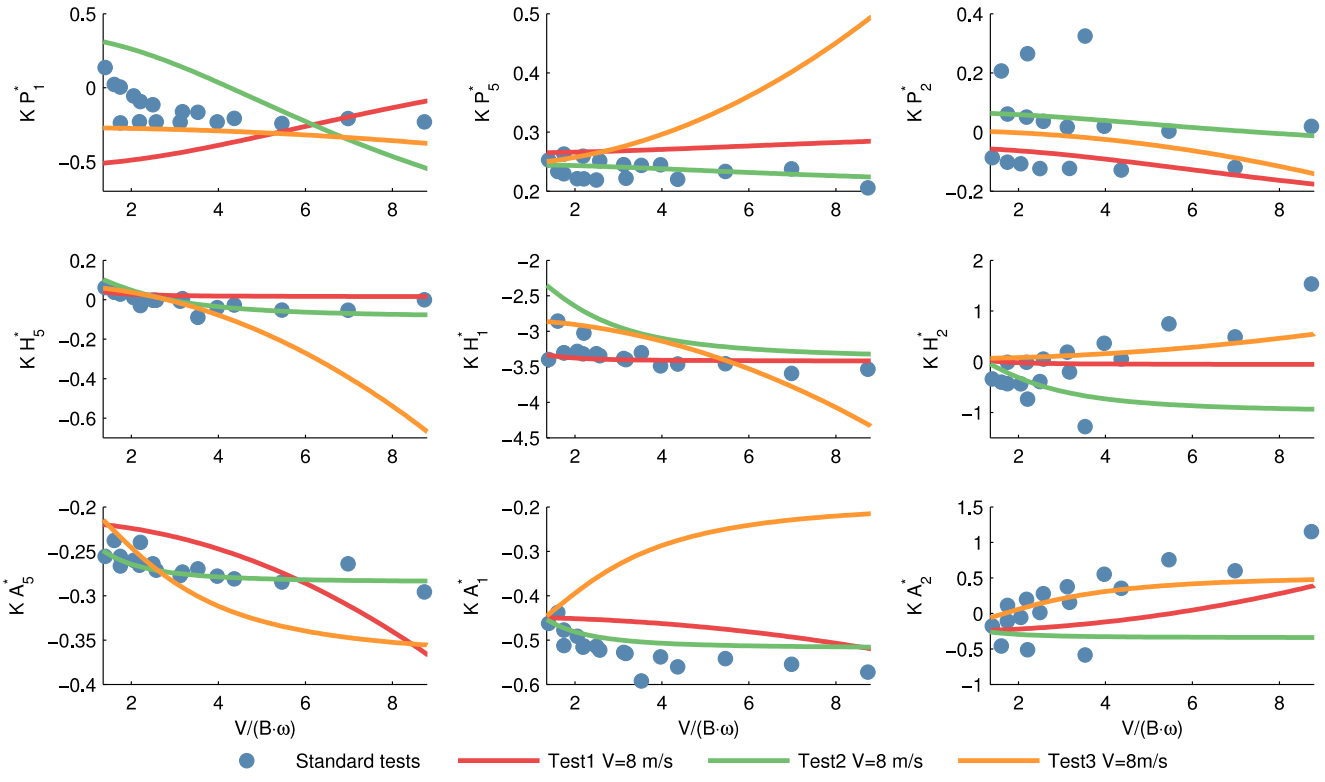

Fig. 8. Aerodynamic derivatives, of the twin deck section model, related to the velocities or angular velocities.

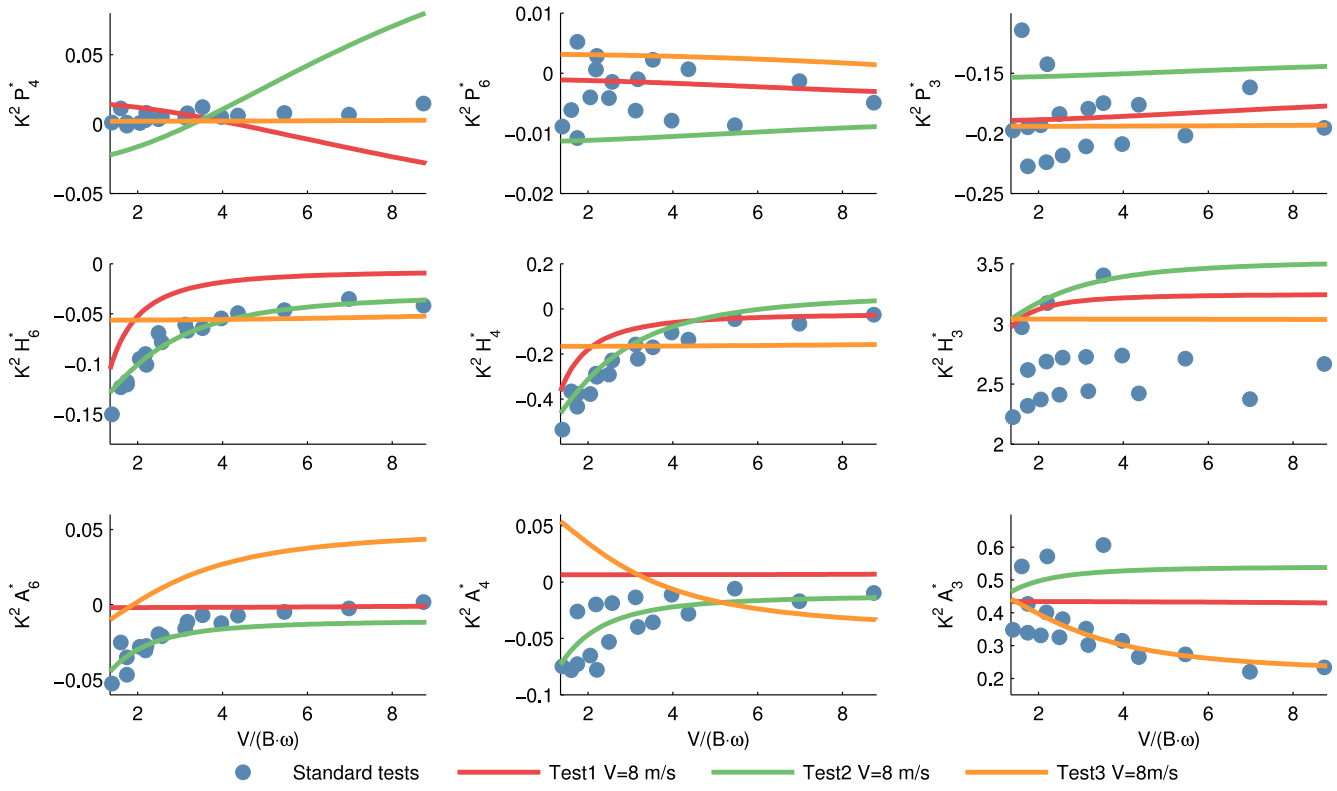

Fig. 9. Aerodynamic derivatives, of the twin deck section model, related to the displacements and rotation.

It is therefore important to emphasize that the differences in the obtained rational function coefficients, and consequently the aerodynamic derivatives, do not result from errors in the identification algorithm described in this paper but it rather indicates that more advanced nonlinear models needs to be applied. There exists several nonlinear models that it is worth to consider, for instance (Diana et. al., 2008; Wu and Kareem, 2014), but this is considered to be out of the scope of this paper and the twin deck section is therefore not discussed further in this paper.

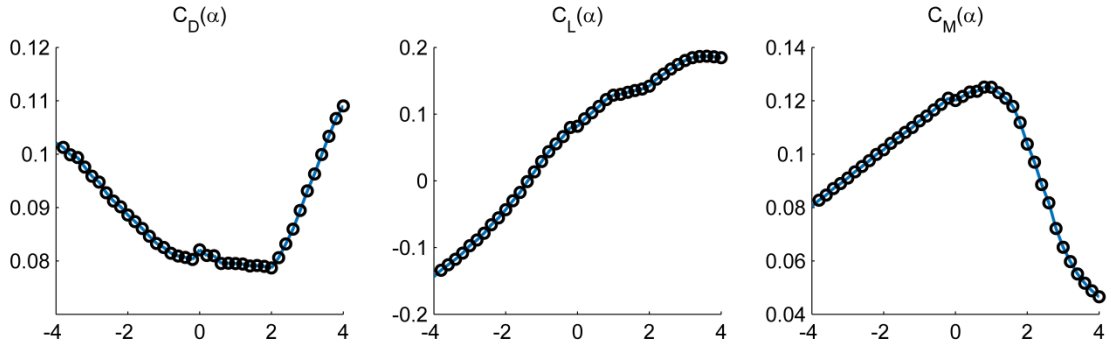

Fig 10. Static load coefficients of the twin deck section model.

4.2 Validation of the rational function coefficients

It is important to ensure that the identified model describes the self-excited forces well for all of the time series and not just the particular time series used to identify the coefficients. It is therefore necessary to validate the model using validation data that have not been used to determine the coefficients. New sets of motion histories, Test 1^*, Test 2^*, and Test 3^*, were therefore obtained assuming the same spectra as in Tests 1, 2 and 3, respectively. The measured aeroelastic forces induced on the Hardanger Bridge and rectangular BD10 section models were compared with the predicted aeroelastic forces, calculated using the identified rational function coefficients, shown in Table 3 and Table 4. Fig. 11 and Fig. 12 display selected time series of the measured and predicted self-excited forces induced during execution of the random motion series for the chosen tests , corresponding to the tabularized data with bold font in Table 3 and Table 4. The self-excited forces were calculated by constructing a state space model from the rational function coefficients and utilizing Eq. (5), for example, similarly to (Bera and Chandiramani, 2016; Chen et al., 2000a, 2000c; Siedziako and Øiseth, 2017a; Øiseth et al., 2012).

Test	V [m/s]	Drag		Lift		Pitch	
		ρ_{xy}	σ_x / σ_y	ρ_{xy}	σ_x / σ_y	ρ_{xy}	σ_x / σ_y
Test 1	10	0.769	0.835	0.997	1.003	1.00	1.006
Test 2	8	0.588	0.639	0.994	1.001	0.999	1.007
Test 3	10	0.788	0.793	0.997	1.003	0.999	1.007
Test 1^*	10	0.654 (0.811)	0.701 (0.817)	0.994 (0.995)	1.001 (0.996)	0.999 (0.999)	1.004 (1.004)
Test 3^*	10	0.663 (0.807)	0.586 (0.804)	0.991 (0.996)	0.985 (0.997)	0.999 (0.999)	1.007 (1.005)
Test 1^*	8	0.542 (0.615)	0.998 (0.614)	0.997 (0.997)	0.976 (0.997)	1.00 (1.00)	1.004 (1.003)
Test 3^*	**8**	**0.586 (0.886)**	**0.510 (0.899)**	**0.995 (0.997)**	**0.953 (1.002)**	**0.999 (1.00)**	**1.008 (1.007)**
Test 1^*	4	0.165 (0.444)	0.622 (0.449)	0.916 (0.929)	0.830 (0.925)	0.981 (0.991)	1.016 (0.992)
Test 3^*	4	0.287 (0.352)	0.319 (0.355)	0.922 (0.926)	0.819 (0.923)	0.996 (0.996)	1.034 (0.999)

Table 3. Correlation coefficient and standard deviation ratio between the measured self-excited forces induced on the Hardanger Bridge section model and those predicted with the identified rational function coefficients. The values in the brackets show the possible best fit obtained, when applying the identification algorithm directly to the considered time series.

Test	V [m/s]	Drag		Lift		Pitch	
		ρ_{xy}	σ_x / σ_y	ρ_{xy}	σ_x / σ_y	ρ_{xy}	σ_x / σ_y
Test 1	8	0.490	0.508	0.999	1.004	0.999	1.010
Test 2	8	0.419	0.423	0.998	1.005	0.999	1.011
Test 3	8	0.356	0.353	0.999	1.005	0.999	1.010
Test 1^*	10	0.530 (0.540)	0.378 (0.538)	0.999 (0.999)	1.001 (1.008)	0.999 (0.999)	1.016 (0.996)
Test 2^*	10	0.136	0.363	0.999	1.009	0.999	1.018

		(0.343)	(0.344)	(0.999)	(1.009)	(0.999)	(0.995)
Test 3*	10	0.132	0.603	0.998	1.001	0.998	1.016
		(0.179)	(0.178)	(0.998)	(1.007)	(0.998)	(0.994)
Test 1*	4	0.844	0.578	0.987	1.007	0.993	0.978
		(0.899)	(0.894)	(0.995)	(0.989)	(0.997)	(1.001)
Test 2*	**4**	**0.902**	**0.231**	**0.992**	**1.025**	**0.984**	**0.988**
		(0.936)	**(0.935)**	**(0.997)**	**(1.004)**	**(0.997)**	**(1.005)**
Test 3*	4	-0.350	0.304	0.984	1.068	0.995	0.993
		(0.772)	(0.765)	(0.996)	(0.991)	(0.998)	(1.001)

Table 4. Correlation coefficient and standard deviation ratio between the measured self-excited forces induced on the rectangular BD10 section model and those predicted with the identified rational function coefficients. The values given in the brackets show the possible best fit obtained, when applying the identification algorithm directly to the considered time series

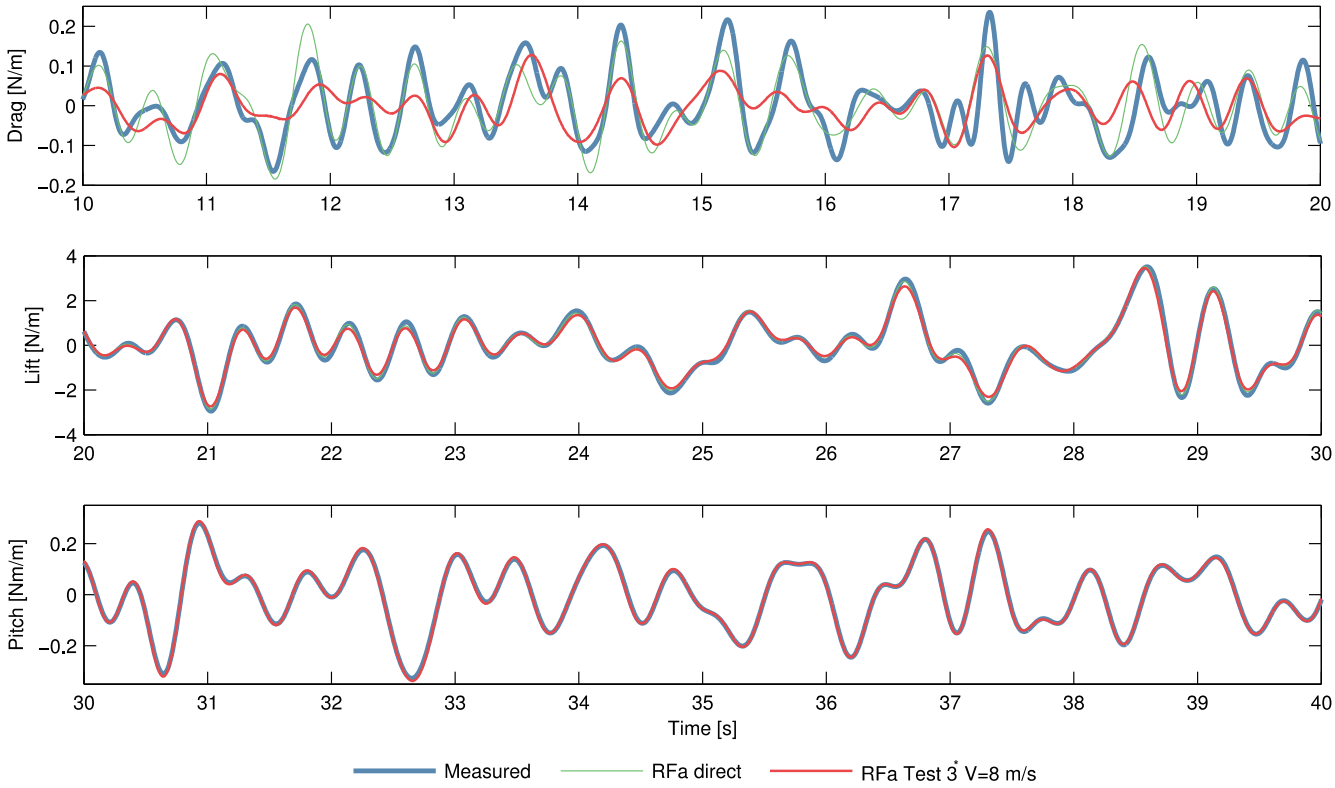

Fig. 11. Comparison of the measured and predicted self-excited forces for Test 3* of the Hardanger Bridge section model, with velocity V=8 m/s. Forces were predicted with the rational function coefficient identified based on Test 3 with velocity 10 m/s (red) and obtained by applying the identification procedure to the data measured in this test (green).

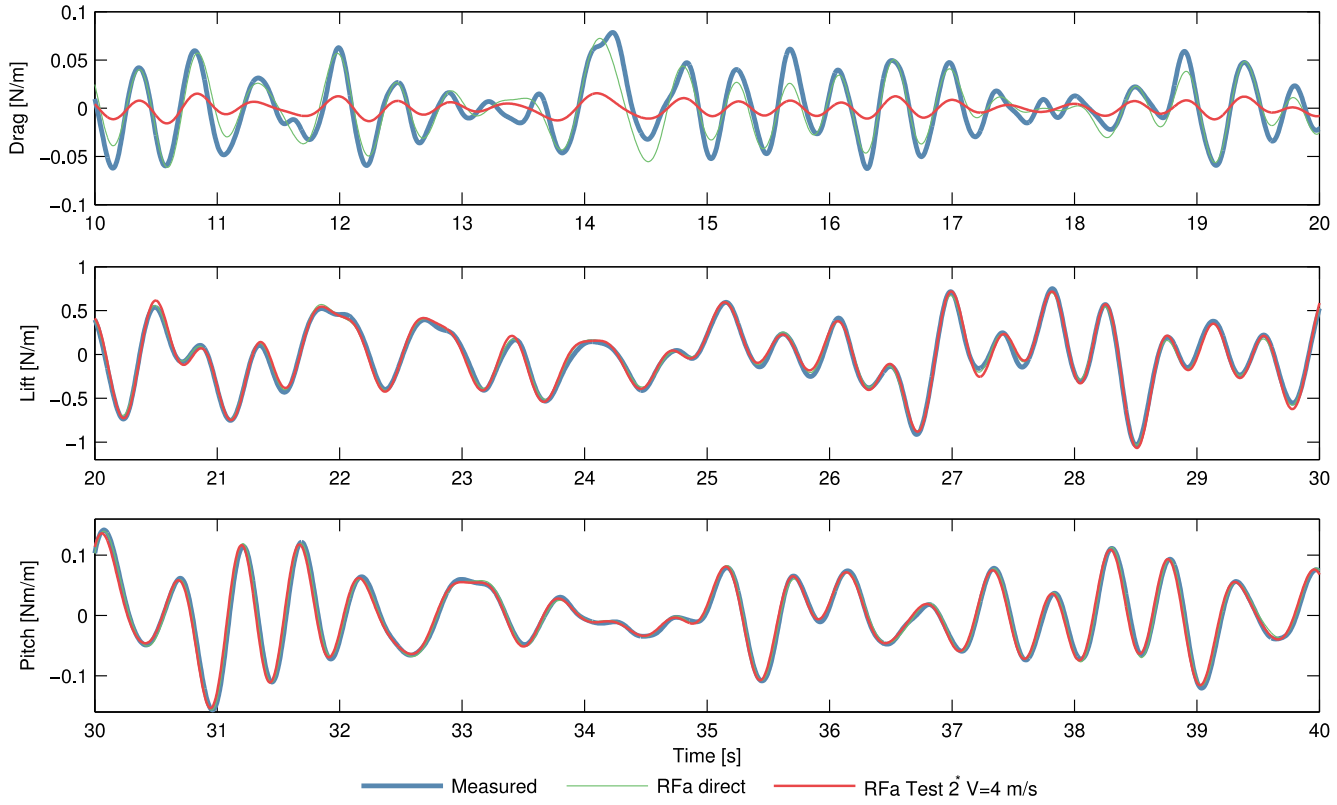

Fig. 12. Comparison of the measured and predicted self-excited forces for Test 2* of the rectangular BD10 section model, with velocity V=4 m/s. Forces were predicted with a use of the rational function coefficient identified based on Test 2 with velocity 8 m/s (red) and obtained by applying the identification procedure to the data measured in this test (green).

The data presented in Table 3 and Table 4, show that the self-excited lift and pitch can be closely reproduced using the identified rational function coefficients by applying random motions, when considering different motion histories and different wind conditions. In all performed tests, the correlation coefficient between the measured and predicted aeroelastic lift and pitch is greater than 0.91 and 0.97 for the Hardanger Bridge and rectangular section models, respectively, proving that the identification results are accurate. Achieving so high accuracy for the test at 4 m/s illustrate that the identified models are very robust since this reduced velocity range was not covered by the applied motion and the mean wind velocities in the tests used to determine the coefficients. For the self-excited drag, however, the predictions do not closely match the measurements in most of the performed tests. This can be attributed, in part, to the presence of nonlinear effects, which can dominate the signal, as shown in (Siedziako and Øiseth, 2017b; Xu et al., 2016), especially when considering the large motion amplitudes such as those forced in Test 3 and Test 3*. Moreover, the aeroelastic properties that determine the magnitude of the self-excited drag are motion-dependent for both the Hardanger Bridge and rectangular section models. It has been shown that by

applying the identification algorithm directly on the considered time series, the predictions of the drag force can drastically improve. This improvement is especially clear during the tests at higher wind speeds in the case of the Hardanger Bridge section model (Fig. 11) and lower wind speeds in the case of the rectangular BD10 section (Fig. 12), when the self-excited drag behaves mostly linear. However, the self-excited drag is often considered to be of low importance. The aerodynamic derivatives defining this force component are rarely obtained through the wind tunnel tests and are more frequently determined by applying the quasi-steady theory and static load coefficients. Therefore, it is difficult to assess how the nonlinearities of the drag force observed in this study influence the overall behavior of the bridge.

5 Conclusion

A new approach for the identification of rational functions and aerodynamic derivatives of bridge deck section models have been presented in this paper. It has been shown that a full set of aerodynamic derivatives, covered in a wide range of reduced velocities, can be extracted by only a few wind tunnel tests in which the section model is subjected to random vibrations. The proposed method has been applied to 3 different section models: a section corresponding to Hardanger Bridge, a rectangular and a twin box girder. The induced self-excited forces were measured during a series of wind tunnel tests, where all the models were forced into 3-DoF's random motions, considering different vibration amplitudes and wind velocities. The identified aerodynamic derivatives were compared with the data obtained by performing standard forced vibration tests. The following conclusions were deduced from the results:

- It has been shown that the identification procedure described in this paper provides very accurate results, if the aerodynamic derivatives of the tested section model can be considered functions of reduced velocity only. For the 8 most influential aerodynamic derivatives for the Hardanger Bridge rectangular section models, nearly an exact match with the data obtained by applying the standard forced vibration tests is observed.
- The approach presented in this study leads to a substantial reduction of the time, resources and in turn costs associated with extracting aerodynamic derivatives and rational functions from wind tunnel test on section models. It should however be noted that an advanced forced vibration setup is required.
- The identified rational function coefficients were successfully used to predict the self-excited lift and pitch induced during random motions at different wind speeds. However, the self-excited drag was underestimated due to its nonlinear behavior and motion dependency.
- Nonlinearities in the recorded self-excited forces were observed for all of the examined section models. The drag component experiences significant higher-order contributions that become stronger at lower and higher wind velocities in

the case of the Hardanger Bridge and rectangular sections, respectively. For the twin box girder, not only the drag but also the pitch is prone to nonlinear effects.

- In this study, the aerodynamic derivatives related to the horizontal motion were captured with lower accuracy, since the forces induced by the horizontal motion herein were of 1 to 2 orders of magnitude smaller than the forces induced by the vertical or torsional vibrations, and therefore their importance was marginal. It is expected, however, that choosing a proper scaling between the horizontal, vertical and torsional vibrations or that testing each of the DoF's separately will provide a significant improvement in the estimation of the aerodynamic derivatives related to horizontal motion.
- The assumptions that aerodynamic derivatives are functions of only the reduced velocity and uniquely define the aeroelastic properties of the section model is not valid for the twin deck type geometry tested here, since the aerodynamic derivatives identified for the twin deck section model are clearly motion-dependent.

Acknowledgment

This research was conducted with financial support from the Norwegian Public Roads Administration. The authors gratefully acknowledge their support.

References

Adaramola, M.S., Krogstad, P.-Å., 2009. Model Tests of a Horizontal Axis Wind Turbine in Yawed Condition, in: European Offshore Wind Conference and Exhibition. Stockholm.

Andersen, M.S., Johansson, J., Brandt, A., Hansen, S.O., 2016. Aerodynamic stability of long span suspension bridges with low torsional natural frequencies. Eng. Struct. 120, 82–91. doi:10.1016/j.engstruct.2016.04.025

Andersen, M.S., Læsø, J.R., Lenius, M., Johansson, J., 2015. Non-flutter design principle for twin boxes, in: 14th International Conference on Wind Engineering.

Bera, K.K., Chandiramani, N.K., 2016. Time Domain Flutter Speed Analysis of Cable Stayed Bridge. Procedia Eng. 12th Int. Conf. Vib. Probl. ICOVP 2015 Time 144, 917–927. doi:10.1016/j.proeng.2016.05.117

Boonyapiny, V., Miyata, T., Yamada, H., 1999. Advanced aerodynamic analysis of suspension bridges by state- space approach. J. Struct. Eng. 125, 1357–1366.

Cao, B., Sarkar, P.P., 2012. Identification of Rational Functions using two-degree-of-freedom model by forced vibration method. Eng. Struct. 43, 21–30. doi:10.1016/j.engstruct.2012.05.003

Chen, X., Kareem, A., 2003. Aeroelastic Analysis of Bridges: Effects of Turbulence and Aerodynamic Nonlinearities. J. Eng. Mech. 129, 885–895. doi:10.1061/(ASCE)0733-9399(2003)129:8(885)

Chen, X., Matsumoto, M., Kareem, A., 2000a. Time domain flutter and buffeting response analysis of bridges. J. Eng. Mech. 7–16.

Chen, X., Matsumoto, M., Kareem, A., 2000b. Aerodynamic Coupling Effects on flutter and buffeting of bridges. J. Eng. Mech. 17–26.

Chen, X., Matsumoto, M., Kareem, A., 2000c. Time Domain Flutter and Buffeting Response Analysis of Bridges. J. Eng. Mech. 126, 7–16. doi:10.1061/(ASCE)0733-9399(2000)126:1(7)

Chen, Z.Q., Yu, X.D., Yang, G., Spencer, B.F., 2005. Wind-Induced Self-Excited Loads on Bridges. J. Struct. Eng. 131, 1783–1793. doi:10.1061/(ASCE)0733-9445(2005)131:12(1783)

Chowdhury, A.G., Sarkar, P.P., 2005. Experimental identification of rational function coefficients for time-domain flutter analysis. Eng. Struct. 27, 1349–1364. doi:10.1016/j.engstruct.2005.02.019

Diana, G., Resta, F., Rocchi, D., 2008. A new numerical approach to reproduce bridge aerodynamic non-linearities in time domain. J. Wind Eng. Ind. Aerodyn. 96, 1871–1884. doi:10.1016/j.jweia.2008.02.052

Diana, G., Resta, F., Zasso, a., Belloli, M., Rocchi, D., 2004. Forced motion and free motion aeroelastic tests on a new

concept dynamometric section model of the Messina suspension bridge. J. Wind Eng. Ind. Aerodyn. 92, 441–462. doi:10.1016/j.jweia.2004.01.005
Diana, G., Rocchi, D., Belloli, M., 2015. Wind tunnel : a fundamental tool for long-span bridge design. Struct. Infrastruct. Eng. Maintenance, Manag. Life-Cycle Des. Perform. 11, 533–555. doi:10.1080/15732479.2014.951860
Estimation, Represent Nonlinear Dynamics Using MATLAB File for Grey-Box [WWW Document], 2017. URL http://se.mathworks.com/help/ident/examples/represent-nonlinear-dynamics-using-matlab-file-for-grey-box-estimation.html
Fenerci, A., Øiseth, O., 2017. Measured buffeting response of a long-span suspension bridge compared with numerical predictions based on design wind spectra. J. Struct. Eng. 143, 4017131. doi:10.1061/(ASCE)ST.1943-541X.0001873
Fenerci, A., Øiseth, O., 2015. Full-ScaleMeasurements on the Hardanger Bridge During StrongWinds, in: Dynamics of Civil Structures, Volume 2, Conference Proceedings of the Society for Experimental Mechanics Series. pp. 237–245. doi:10.1007/978-3-319-15209-7
Fenerci, A., Øiseth, O., Rönnquist, A., 2017. Long-term monitoring of wind field characteristics and dynamic response of a long-span suspension bridge in complex terrain. Eng. Struct. 147, 269–284. doi:10.1016/j.engstruct.2017.05.070
Fuller, R.G., Lang, C.R., Lang, R.H., 2000. Twin views of the Tacoma Narrows Bridge collapse. American Association of Physics Teachers.
Høgsberg, J.R., Krabbenhøft, J., Krenk, S., 2000. State Space Representation of Bridge Deck Aeroelasticity, in: J. Hellesland, H. Osnes, G. Skeie (Eds.), Proceedings of the 13th Nordic Seminar on Computational Mechanics, Oslo. pp. 109–112.
Jain, A., Jones, N.P., Scanlan, R.H., 1996. Coupled Flutter and Buffeting Analysis of Long-Span Bridges. J. Struct. Eng. 122, 716–725. doi:10.1061/(ASCE)0733-9445(1996)122:7(716)
Karpel, M., 1981. Design for active and passive flutter suppression and gust alleviation.
Katsuchi, B.H., Jones, N.P., Scanlan, R.H., 1999. Multimode coupled flutter and buffeting analysis of the Akashi-Kaikyo Bridge. J. Struct. Eng. 125, 60–70. doi:0733-9445
Keesman, K.J., 2011. System Identification An Itroduction. Springer London, New York. doi:10.1007/978-0-85729-522-4
Lim, R.K., Longman, R.W., 1998. State-Space System Identification with Identified Hankel Matrix, Department of Mechanical and Aerospace Engineering Technical Report No. 3045.
Ljung, L., 1987. System Identification: Theory for User. Automatica. doi:10.1016/0005-1098(89)90019-8
Matsuda, K., Cooper, K.R., Tanaka, H., Tokushige, M., Iwasaki, T., 2001. An investigation of Reynolds number effects on the steady and unsteady aerodynamic forces on a 1:10 scale bridge deck section model. J. Wind Eng. Ind. Aerodyn. 89, 619–632. doi:10.1016/S0167-6105(01)00062-9
Mishra, S.S., Kumar, K., Krishna, P., 2008. Multimode flutter of long-span cable-stayed bridge based on 18 experimental aeroelastic derivatives. J. Wind Eng. Ind. Aerodyn. 96, 83–102. doi:10.1016/j.jweia.2007.03.006
Neuhaus, C., Mikkelsen, O., Bogunovic Jakobsen, J., Höffer, R., Zahlten, W., 2009. Time domain representations of unsteady aeroelastic wind forces by rational function approximations, in: EACWE 5. Florence.
Roger K. L., 1977. Airplane Math Modeling and Active Aeroelastic Control Design[C]. Agard-Cp-228.
Sarkar, P.P., Caracoglia, L., Haan, F.L., Sato, H., Murakoshi, J., 2009. Comparative and sensitivity study of flutter derivatives of selected bridge deck sections, Part 1: Analysis of inter-laboratory experimental data. Eng. Struct. 31, 158–169. doi:10.1016/j.engstruct.2008.07.020
Sarkar, P.P., Chowdhury, a. G., Gardner, T.B., 2004. A novel elastic suspension system for wind tunnel section model studies. J. Wind Eng. Ind. Aerodyn. 92, 23–40. doi:10.1016/j.jweia.2003.09.036
Scanlan, R.H., Jones, N.P., Lorendeaux, O., 1997. Comparison of taut-strip and section-model-based approaches in long-span bridge aerodynamics. J. Wind Eng. Ind. Aerodyn. 72, 275–287. doi:10.1016/S0167-6105(97)00250-X
Scanlan, R.H., Tomko, J., 1971. Airfoil and bride deck flutter derivaitves. J. Eng. Mech. Div. 97, 1717–33.
Schön, T.B., Wills, A., Ninness, B., 2011. System identification of nonlinear state-space models. Automatica 47, 39–49. doi:10.1016/j.automatica.2010.10.013
Siedziako, B., Øiseth, O., 2017a. Identification of Rational Functions with a forced vibration technique using random motion histories, in: ICESD2017, Reykjavík.
Siedziako, B., Øiseth, O., 2017b. Modeling of self-excited forces during multimode flutter: numerical predictions versus wind tunnel measurements. Submitt. to J. Wind Struct.
Siedziako, B., Øiseth, O., Rønnquist, A., 2017a. An enhanced forced vibration rig for wind tunnel testing of bridge deck section models in arbitrary motion. J. Wind Eng. Ind. Aerodyn. 164, 152–163. doi:10.1016/j.jweia.2017.02.011
Siedziako, B., Øiseth, O., Rønnquist, A., 2017b. Wind Tunnel Testing of Bridge Deck Section Models with a New Forced Vibration Rig, in: Proceedings of The 7th European and African Conference on Wind Engineering, Liège.
Siedziako, B., Øiseth, O., Rönnquist, A., 2016. A new setup for section model tests of bridge decks, in: Proceedings of 12th UK Conference on Wind Engineering. Nottingham.
Singh, L., Jones, N.P., Scanlan, R.H., Lorendeaux, O., 1996. Identification of lateral flutter derivatives of bridge decks. J. Wind Eng. Ind. Aerodyn. 60, 81–89.

Skyvulstad, H., Siedziako, B., Øiseth, O., 2017. An Experimental Study of Self-excited Forces for Twin Deck Section Models, in: Proceedings of The 7th European and African Conference on Wind Engineering, Liège.
Wardlaw, R.L., 1980. Sectional versus full model wind tunnel testing of bridge road decks. Proc. Indian Acad. Sci. Sect. C Eng. Sci. 3, 177–198. doi:10.1007/BF02861559
Wu, T., Kareem, A., 2014. Simulation of nonlinear bridge aerodynamics: A sparse third-order Volterra model. J. Sound Vib. 333, 178–188. doi:10.1016/j.jsv.2013.09.003
Xu, F.Y., Wu, T., Ying, X.Y., Kareem, A., 2016. Higher-order Self-Excited Drag Forces on Bridge Decks. J. Eng. Mech. 142, 1–11. doi:10.1061/(ASCE)EM.1943-7889.0001036
Yang, Y., Zhou, R., Ge, Y., Mohotti, D., Mendis, P., 2015. Aerodynamic instability performance of twin box girders for long-span bridges. J. Wind Eng. Ind. Aerodyn. 145, 196–208. doi:10.1016/j.jweia.2015.06.014
Zasso, A., 1996. Flutter derivatives: Advantages of a new representation convention. J. Wind Eng. Ind. Aerodyn. 60, 35–47. doi:10.1016/0167-6105(96)00022-0
Zasso, A., Belloli, M., Argentini, T., Flamand, O., Knapp, G., Grillaud, G., Klein, J., Virlogeux, M., Ville, V. De, 2014. Third Bosporus Bridge aerodynamics: Sectional and fulll-aerolastic model testing, in: Istanbul Bridge Conference.
Zhang, X., Brownjohn, J.M.W., 2005. Some considerations on the effects of the P-derivatives on bridge deck flutter. J. Sound Vib. 283, 957–969. doi:10.1016/j.jsv.2004.05.031
Øiseth, O., 2015. Modelling aerodynamic self-excited forces by means of state space models, in: Lecture Note.
Øiseth, O., Rönnquist, A., Sigbjörnsson, R., 2012. Finite element formulation of the self-excited forces for time-domain assessment of wind-induced dynamic response and flutter stability limit of cable-supported bridges. Finite Elem. Anal. Des. 50, 173–183. doi:10.1016/j.finel.2011.09.008
Øiseth, O., Rönnquist, A., Sigbjörnsson, R., 2010. Simplified prediction of wind-induced response and stability limit of slender long-span suspension bridges, based on modified quasi-steady theory: A case study. J. Wind Eng. Ind. Aerodyn. 98, 730–741. doi:10.1016/j.jweia.2010.06.009